American Mineralogist, Volume 93, pages 1317–1325, 2008

Thermal behavior and structural transformation in the chabazite-type zeolite willhendersonite, $KCaAl_3Si_3O_{12}\cdot 5H_2O$

R.X. Fischer,[1,*] V. Kahlenberg,[2] C.L. Lengauer,[3] and E. Tillmanns[3]

[1]Universität Bremen, Fachbereich Geowissenschaften, Klagenfurter Strasse, D-28359 Bremen, Germany
[2]Universität Innsbruck, Institut für Mineralogie und Petrographie, Innrain 52, A-6020 Innsbruck, Austria
[3]Universität Wien-Geozentrum, Institut für Mineralogie und Kristallographie, Althanstrasse 14, A-1090 Wien, Austria

Abstract

Single crystals of the chabazite-type zeolite mineral willhendersonite, $KCaAl_3Si_3O_{12}\cdot 5H_2O$ (from Bellerberg, eastern Eifel district, Germany), were studied by X-ray diffraction methods between 100 and 500 K. The zeolite shows a phase transition from triclinic to rhombohedral symmetry between 350 and 375 K under dry nitrogen and between 450 and 475 K under humid air. Under these conditions, the unit-cell parameters change from $P\bar{1}$ at 350 K [*a*, *b*, *c* (Å); α, β, γ (°); *V* (Å^3) = 9.210, 9.210, 9.405; 92.75, 92.80, 90.80; 795.8] to $R\bar{3}$ at 375 K (*a* = 9.380 Å, α = 91.40°, *V* = 824.5 Å^3), and from $P\bar{1}$ at 450 K [*a*, *b*, *c* (Å); α, β, γ (°); *V* (Å^3) = 9.215, 9.215, 9.415; 92.65, 92.85, 90.75; 797.5] to $R\bar{3}$ at 475 K (*a* = 9.375 Å, α = 91.35°, *V* = 823.8 Å^3), respectively. The crystal structures were refined based on X-ray diffraction data collected at room temperature [$P\bar{1}$; *a*, *b*, *c* (Å); α, β, γ (°); *V* (Å^3) = 9.248(5), 9.259(5), 9.533(5); 92.313(5), 92.761(5), 89.981(5); 814.7(8)], at 373 K [$P\bar{1}$; *a*, *b*, *c* (Å); α, β, γ (°); *V* (Å^3) = 9.205(5), 9.231(5), 9.442(5); 92.550(5), 93.086(5), 90.519(5); 800.3(8)], and at 423 K [$R\bar{3}$, *a* = 9.411(4) Å, α = 91.48(1)°, *V* = 832.7(6) Å^3]. Upon heating, the elliptical 8-rings of willhendersonite expand to a triangular shape in the rhombohedral structure with upper and lower rings in the double 6-ring (D6R) twisted by 60° to each other corresponding to the center of symmetry in the center of the D6R. The changes in the framework are accompanied by migration of cations, partly assuming unfavorably low coordinations in the high temperature structure due to the loss of H_2O molecules. Rehydration at room temperature yields the triclinic structure of willhendersonite, although the single crystals become polysynthetically twinned.

Keywords: Willhendersonite, chabazite, zeolite, dehydration, crystal structure, nonambient conditions

Introduction

The rare zeolite mineral willhendersonite (*will* hereafter) with the general composition $K_xCa_{1.5-0.5x}(Al_3Si_3O_{12})\cdot 5H_2O$ (idealized $KCaAl_3Si_3O_{12}\cdot 5H_2O$) was first described by Peacor et al. (1984), who studied specimens from a quarry near San Venanzo (Terni province, Italy) and from the Quaternary volcanic rocks of the Ettringer Bellerberg near Mayen (Eifel area, Germany). Structural investigations by Tillmanns and Fischer (1982) and Tillmanns et al. (1984) on single crystals from the German locality revealed the close structural relationship to chabazite, $CaAl_2Si_4O_{12}\cdot 6H_2O$, which has the same framework topology with framework type code CHA (Baerlocher and McCusker 2007). A further occurrence was reported by Walter and Postl (1984) from the nephilinites of the Stradner Kogel near Wilhelmsdorf (Styria, Austria), and a chemical and crystallographic description of a Ca-rich *will* from Colle Fabbri, a second locality within the volcanic rocks of the Terni province, was given by Vezzalini et al. (1997).

The geometry of the triclinic unit cell of *will* ($P\bar{1}$) with cell parameters *a* ~ 9.20 Å, *b* ~ 9.21 Å, *c* ~ 9.50 Å, α ~ 92.3°, β ~ 92.7°, and γ ~ 90.0° is close to the reported idealized rhombohedral cell dimensions of chabazite with *a* ~ 9.41 Å and α ~ 94.3° (Gottardi and Galli 1985). In contrast to the average chabazite structure ($R\bar{3}m$) with a random cation distribution over the tetrahedrally coordinated framework sites, the complete Al/Si ordering in the case of *will* leads to a lowering of the topochemical symmetry to space group $R\bar{3}$. A similar feature is commonly observed for various forms of the synthetic $AlPO_4$ analogues (e.g., Feng et al. 1997) with their corresponding Al/P ordering. The additional symmetry reduction in the structure of *will* to the observed triclinic form is caused mainly by a pronounced elliptical distortion of the double 6-rings [D6R, *hpr* ($4^6 6^2$) units after Smith 2000], the main structural building unit of the chabazite-type framework. Further contributions come from a nonrhombohedral distribution of the nonframework cations and molecules over three main crystallographic site clusters. In a similar manner, it is well known from optical (Becke 1880; Akizuki 1981) and X-ray investigations (Smith et al. 1964) that the real chabazite structure is triclinic, possibly as a result of a random arrangement of domains with high Al/Si order (Mazzi and Galli 1983). Other chabazite-type compounds with triclinic symmetry are reported for as-synthesized forms of $AlPO_4$-34 (Simmen 1992; Harding and Kariuki 1994), $GaPO_4$-34 (Schott-Darie et al. 1994), and

* E-mail: rfischer@uni-bremen.de

UT-6 (Oliver et al. 1997). CoAPO-44 and CoAPO-47 are also described in the triclinic space group $P\bar{1}$ (Bennett and Marcus 1988) but with a unit cell three times the volume of *will*, thus crystallizing in a subgroup of $R\bar{3}m$ with a symmetry reduction of index 18, whereas *will* has a symmetry reduction of index 6 (Baur and Fischer 2000).

Like chabazite, all *will* crystals of practical size exhibit twinning. From the Terni localities twinning around the pseudo rhombohedral axis is reported, which typically leads to the so-called "trellis-like" aggregates (Peacor et al. 1984). For the German locality, a different twin type was found to be more abundant, which can be easily recognized by viewing the platelets under the polarizing microscope parallel to [001] through the diagonal boundary of the twinned domains. Based on spindle stage investigations and crystallographic considerations, Sieber (1989) concluded that this twin type can be explained either by reflection across (110) or by rotation about [1$\bar{1}$0]. As twinning on this mirror plane would require a bending of the D6R, the more likely rotation type twin-law was assumed for these *will* samples. Furthermore, Sieber (1989) observed in subsequent investigations that within the *will* platelets the difference of the extinction angles of the twinned domains (4.8° at 297 K) discontinuously increases at elevated temperatures from 7.2 to 19.8° (353–393 K) and suddenly disappears between 450 and 455 K (Fig. 1). Upon cooling, the crystal disintegrates into polysynthetic twin domains. The most reasonable explanation for this thermal behavior was a first-order phase transition resulting in a true rhombohedral symmetry for dehydrated *will*.

A detailed description of these processes, however, was prevented by experimental restrictions and the quality of the sample crystals. Therefore, the availability of new excellent sample material from Bellerberg and the enhanced possibilities of using an area detector for the diffraction experiment encouraged us to undertake a detailed temperature-resolved investigation of *will* by means of single-crystal X-ray diffractometry. After preliminary measurements of the nonambient behavior of the unit-cell dimensions of *will*, three single-crystal data sets at room temperature, 373, and 423 K were recorded to provide a basis for a structural characterization of the dehydration process of this chabazite-type zeolite, and to compare these findings with the interesting optical properties.

Experimental methods

Specimen description and preparation

The crystals were obtained from a suite of *will*-rich samples of a limestone xenolith in the Quaternary volcanic rocks of the Bellerberg near Mayen, eastern Eifel district, Germany. The zeolite can be found in small cavities predominantly filled by gismondine (*gis*), together with light green augite (*aug*), clear needles of apatite (*ap*), and small spherolites of thomsonite (*tho*). The crystallization sequence can be given as *aug* > *gis* > *will* > *ap* + *tho*. *Will* typically occurs as clear platelets flattened on {001}, which were used for the single-crystal investigations (Fig. 2). The "trellis-like" aggregates twinned through rotation around [111] usually known from the occurrence near Terni, Italy, are less abundant. Qualitative and semiquantitative chemical analyses by means of energy-dispersive X-ray analysis using a scanning electron microscope (JEOL) gave Al/Si and K/Ca ratios of 1 ± 0.05 and no indication of any further cation content. Investigations of several crystals up to 0.1 × 0.1 mm^2 with the polarizing microscope revealed that all platelets are diagonally twinned by rotation about [1$\bar{1}$0]. Subsequently, several untwinned fragments of about 0.1 × 0.05 × 0.025 mm^3 were separated for the temperature-resolved experiments. The crystal fragments were mounted on glass fibers (d = 0.04 mm) with a two-component glue (UHU Plus Sofortfest), proven to be heat resistant up to 523 K. To minimize vibrations of the crystals caused by the gas flow during the nonambient measurements, the fibers were stabilized by fixing within quartz-glass capillaries (d = 0.1 mm) up to 1 mm below the crystal. A Reynolds-USGS (Fluid Inc., U.S.A.) heating-cooling device (293 to 453 K, ΔT = 5 ± 1 K) was used for the optical investigations with the polarizing microscope.

Nonambient single-crystal X-ray diffraction

For the purpose of determining unit-cell parameters under dry and relatively humid conditions temperature-resolved single-crystal measurements were performed using a Kappa diffractometer (Nonius, Delft) with Mo$K\alpha$ radiation monochromatized by a polycapillary, parallel beam collimator (IFG, Germany) and equipped with a CCD detector (Princeton Instruments, Trenton). For the low- and high-temperature measurements a liquid nitrogen Cryostream cooler (Oxford Cryosystems, Oxford) based on the work of Cosier and Glazer (1986) and the FR559 air stream heater (Nonius, Delft) were applied, respectively. The temperature stability of the FR559 device as described by Tuinstra and Fraase-Storm (1978),

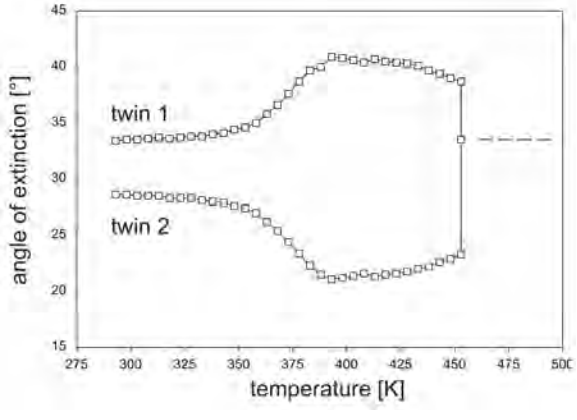

Figure 1. Graphical representation of the optical extinction as a function of temperature of a twinned willhendersonite platelet viewed parallel to [001]. The crystal edges were oriented parallel to 75.5° (100) and 345.5° (010) of the microscope stage and the phase transition occurred between 450 and 455 K.

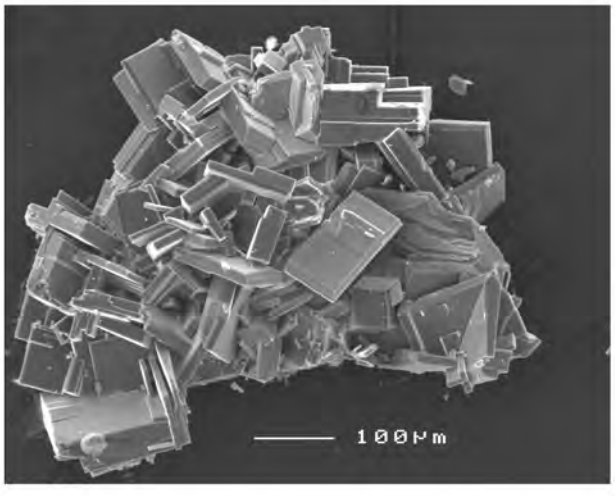

Figure 2. Scanning electron microscope image of tabular willhendersonite crystals from Bellerberg near Mayen (Germany), typically flattened on {001}.

however, is very sensitive to goniometer head movements with temperature deviations up to 20 K. Therefore, after several attempts, the heater was modified for a fixed downward arrangement about 4 mm above the crystal alignment position. This heating device allowed unrestricted movements of the goniometer head under reliable nonambient measurement conditions with $\Delta T \pm 5$ K up to 623 K. As the air stream is stabilized by passing through a partly filled water chamber, the FR599 provides a water vapor pressure of approximately 27 mbar at 297 K.

For these preliminary temperature-resolved unit-cell parameter refinements, measurements under the dry N_2 of the Cryostream cooler (100–375 K, $\Delta T = 25$ K) and under the relative humidity of the FR559 heating device (300–500 K, $\Delta T = 25$ K) were performed. At each temperature the crystals were allowed to equilibrate for 15 min, followed by realignment and an identical data collection of 10 frames of an ω-scan (Δω: 2°, *t*: 90 s, ψ: 57°) with a crystal-to-detector distance of 35 mm. The unit-cell parameters of *will* under nonambient conditions, together with available literature data, are listed in Table 1.

Single-crystal structure refinement

Single-crystal data collections for the crystal structure analyses were performed with a STOE imaging plate diffractometer system (IPDS) equipped with an in-house heating device. To evaluate the thermal behavior of *will* under these conditions, the temperature was raised stepwise until the phase transition was observed and completed at 423 K, which is in agreement with the temperature-resolved results under dry nitrogen described above.

The IPDS single-crystal data collections for the structure refinements were started with unheated *will* at room temperature (WIL-RT), followed by a measurement at 373 K (WIL-373) close below the phase transition temperature, and a final data collection at 423 K (WIL-423). Optical examinations of the heat treated, rehydrated crystals at ambient conditions showed the occurrence of polysynthetic twinning, thus preventing a single-crystal investigation of the rehydrated form of *will*. Data reduction, including intensity integrations, Lorentz, and polarization corrections, were carried out with the STOE IPDS software. No absorption correction was applied and all intensities were integrated and scaled in space group *P*1. The space groups of the triclinic (WIL-RT, WIL-373) and rhombohedral (WIL-423) forms were determined by reflection statistics to be $P\bar{1}$ and $R\bar{3}$, respectively. Single-crystal structure refinements on F^2 were performed with the program SHELXL-97 (Sheldrick 1997), and crystal structure drawings and distance and angle calculations were performed with STRUPLO (Fischer and Messner 2007) as part of the BRASS program package (Birkenstock et al. 2007). Radii of nonframework cations and H_2O molecules in the crystal structure drawings are chosen to correspond to about ¼ of their corresponding ionic (Shannon 1976) or molecular radii. The radii of framework O atoms is arbitrarily set to 0.2 Å. The complex scattering factors for neutral atoms were taken from the *International Tables for Crystallography* (Wilson 1992). Further information on the single-crystal structure refinements and other relevant crystallographic data are summarized in Table 2. The refined structural parameters as well as selected interatomic distances and bond angles for the framework and relevant nonframework sites are listed in Tables 3, 4, and 5, respectively.

The refinements were started with the data set of WIL-RT using the coordinates of the framework atoms given by Tillmanns et al. (1984). Subsequent difference-Fourier calculations revealed electron density in the nonframework sites. The distribution of elements on these crystallographic sites was set by crystal chemical considerations accounting for the overall cation content from the chemical analysis. However, site occupancy factors (s.o.f.'s) of the nonframework atoms were allowed to vary independently, resulting in a refined cation and water content closely corresponding to the chemical analyses representing approximately the idealized chemical formula for *will*. Anisotropic displacement parameters were applied to all atoms in the final refinement steps. The data for the partially

TABLE 1. Unit-cell parameters of willhendersonite from Bellerberg, Germany, under nonambient conditions, compared with literature data

T (K)	*a* (Å)	*b* (Å)	*c* (Å)	α (°)	β (°)	γ (°)	*V* (Å³)
Δ*T*-scan under dry conditions							
100(1)	9.155(5)	9.210(5)	9.470(5)	92.15(5)	92.60(5)	90.00(5)	797.1(7)
125(1)	9.160(5)	9.210(5)	9.470(5)	92.20(5)	92.55(5)	90.00(5)	797.5(7)
150(1)	9.160(5)	9.205(5)	9.475(5)	92.25(5)	92.60(5)	90.05(5)	797.5(7)
175(1)	9.165(5)	9.210(5)	9.485(5)	92.35(5)	92.60(5)	90.00(5)	799.1(7)
200(1)	9.170(5)	9.215(5)	9.490(5)	92.40(5)	92.65(5)	90.00(5)	800.4(7)
225(1)	9.175(5)	9.220(5)	9.505(5)	92.35(5)	92.55(5)	90.05(5)	802.6(7)
250(1)	9.190(5)	9.220(5)	9.500(5)	92.40(5)	92.60(5)	90.10(5)	803.4(7)
275(1)	9.200(5)	9.220(5)	9.485(5)	92.45(5)	92.65(5)	90.15(5)	803.0(7)
300(1)	9.200(5)	9.220(5)	9.470(5)	92.50(5)	92.65(5)	90.20(5)	801.6(7)
325(1)	9.205(5)	9.215(5)	9.425(5)	92.80(5)	92.85(5)	90.55(5)	797.5(7)
350(1)	9.210(5)	9.210(5)	9.405(5)	92.75(5)	92.80(5)	90.80(5)	795.8(7)
375(1)	9.380(5)	9.380(5)	9.380(5)	91.40(5)	91.40(5)	91.40(5)	824.5(8)
*	13.426	13.426	15.845	90.0	90.0	120.0	2473.6
Δ*T*-scan under humid conditions							
300(5)	9.215(5)	9.225(5)	9.510(5)	92.35(5)	92.70(5)	90.00(5)	806.9(8)
325(5)	9.210(5)	9.225(5)	9.500(5)	92.40(5)	92.75(5)	90.05(5)	805.5(7)
350(5)	9.215(5)	9.220(5)	9.490(5)	92.40(5)	92.70(5)	90.15(5)	804.7(7)
375(5)	9.210(5)	9.220(5)	9.480(5)	92.40(5)	92.70(5)	90.20(5)	803.4(7)
400(5)	9.210(5)	9.215(5)	9.445(5)	92.65(5)	92.80(5)	90.50(5)	799.7(7)
425(5)	9.210(5)	9.210(5)	9.435(5)	92.70(5)	92.85(5)	90.60(5)	798.4(7)
450(5)	9.215(5)	9.215(5)	9.415(5)	92.65(5)	92.85(5)	90.75(5)	797.5(7)
475(5)	9.375(5)	9.375(5)	9.375(5)	91.35(5)	91.35(5)	91.35(5)	823.8(8)
*	13.414	13.414	15.851	90.0	90.0	120.0	2469.8
500(5)	9.350(5)	9.350(5)	9.350(5)	91.05(5)	91.05(5)	91.05(5)	817.0(8)
*	13.344	13.344	15.895	90.0	90.0	120.0	2451.0
Literature data†							
Terni†	9.138	9.178	9.477	92.31	92.50	90.05	793.4
Terni‡	9.180(3)	9.197(3)	9.440(3)	91.42(2)	91.72(2)	90.05(2)	796.4(5)
Styria§	9.16	9.17	9.49	92.3	92.9	90.4	795.4
Mayen†	9.21(2)	9.23(2)	9.52(2)	92.4(1)	92.7(1)	90.1(1)	807.7(30)
Mayen‖	9.206(2)	9.216(2)	9.500(4)	92.34(3)	92.70(3)	90.12(3)	804.4(4)
Mayen#	9.213(3)	9.213(3)	9.506(3)	92.37(5)	92.67(5)	90.01(5)	805.3(4)
453(10)#	9.2(1)	9.2(1)	9.2(1)	90.2(2)	90.2(2)	90.2(2)	779(15)

Notes: Values from cell-parameter refinements of 10 collected frames with estimated standard deviations in parentheses. Dry conditions: N_2 gas of the Oxford Cryostream cooler. Humid conditions: air with enhanced hydrous pressure of the Nonius FR559 heating device.
* Cell parameters according to hexagonal axes setting.
† Peacor et al. (1984).
‡ Vezzalini et al. (1997).
§ Walter and Postl (1984).
‖ Tillmanns et al. (1984).
Sieber (1989).

TABLE 2. Single-crystal X-ray data collection parameters and structure refinement details for willhendersonite from Bellerberg, Germany, at room temperature (RT), 373, and 423 K

	RT	373 K	423 K rhombohedral setting	423 K hexagonal setting
space group	$P\bar{1}$	$P\bar{1}$	$R\bar{3}_R$	$R\bar{3}_H$
Z	2	2	2	6
a (Å)	9.248(5)	9.205(5)	9.411(4)	13.480(4)
b (Å)	9.259(5)	9.231(5)	9.411(4)	13.480(4)
c (Å)	9.533(5)	9.442(5)	9.411(4)	15.874(4)
α (°)	92.313(5)	92.550(5)	91.48(1)	90
β (°)	92.761(5)	93.086(5)	91.48(1)	90
γ (°)	89.981(5)	90.519(5)	91.48(1)	120
V (Å^3)	814.7(8)	800.3(8)	832.7(6)	2498(1)
No. of measured reflections	14198	13931	14571	
No. of unique reflections	3649	3570	1364	
No. $F_o > 4\sigma(F_o)$	2136	2184	804	
range of h, k, l	$\|h\| \le 12$, $\|k\| \le 12$, $\|l\| \le 12$	$\|h\| \le 12$, $\|k\| \le 12$, $\|l\| \le 12$	$\|h\| \le 12$, $\|k\| \le 12$, $\|l\| \le 12$	
2θ-max (°)	56.3	56.3	56.2	
No. parameters	269	240	88	
No. constraints	0	0	0	
R_{int}/R_σ	0.1066/0.1069	0.0966/0.0893	0.1475 / 0.0836	
$R1/R1 > 4\sigma(F_o)$	0.0935/0.0438	0.0882/0.0445	0.1012 / 0.0479	
w$R2$	0.1117	0.1133	0.1264	
GooF	0.878	0.909	1.084	
min/max ΔeÅ^{-3}	–0.47/0.56	–0.43/0.90	–0.37/0.70	

Notes: STOE IPDS diffractometer with Mo tube (50 kV, 35 mA), λ = 0.71073 Å, crystal size 0.07 × 0.05 × 0.025 mm^3, corrections for Lorentz and polarization effects, no absorption corrections. Values of estimated standard deviations are given in parentheses. F_o = observed structure factor, F_c = calculated structure factor. $R1 = \sum[|F_o| - |F_c|]/\sum|F_o|$, w$R2 = \{\sum[w(F_o^2 - F_c^2)^2]/\sum w(F_o^2)^2\}^{1/2}$, w = 1/[σ$^2F_o^2$ + (0.057*P)2 + 0.0*P], GooF = $\{\sum[w(F_o^2 - F_c^2)^2]/(n - p)\}^{1/2}$, P = [max($F_o^2$,0) + 2*$F_c^2$]/3.

dehydrated WIL-373 were treated similarly, yielding similar cation distributions and, as expected, reduced s.o.f.'s for the water sites. The crystal structure of the dehydrated form of willhendersonite (WIL-423) was solved in $R\bar{3}$ with all reflections obeying rhombohedral symmetry. Refinements followed the procedure described for WIL-RT and WIL-373.

RESULTS AND DISCUSSION

To obtain a preliminary picture of the discontinuous dehydration of *will* (Fig. 1), two temperature-resolved scans under dry nitrogen and under humid air were evaluated (Table 1; Fig. 3). Due to the sensitivity of unit-cell dimensions of zeolite-type phases to environmental changes (e.g., van Reeuwijk 1974), this approach has the potential to provide information on the effects of different partial pressures of H_2O on the dehydration reaction. It is obvious from the plots of Figure 3 that the behavior of the unit-cell parameters in these two temperature scans is similar, but the respective temperature values of the measurements under N_2 are lowered by about 75–100 K from those in humid air. Furthermore c, γ, and V are most responsive to environmental changes (Fig. 3).

In the low-temperature region under N_2, the cell volume of a fully hydrated *will* exhibited an increase in unit-cell volume of 6 Å^3 up to 250 K followed by a negative trend at higher temperatures (250–350 K), which was also observed for *will* under humid air at elevated temperatures (300–450 K). Based on this similar behavior, we expect that *will* dehydrates under dry conditions in the range of 225–250 K (Fig. 3c). A smooth and continuous increase in a and α was observed, whereas b and β did not change significantly between 100 and 300 K (Fig. 3a and 3b).

The observed unit-cell parameters of the untreated WIL-RT agree well with the respective values for the Mayen samples reported in the literature (Table 1). Typical for this occurrence is a significant enlargement of the unit-cell volume in comparison with the data for *will* from the Italian (793.4–796.4 Å^3) and the Austrian (795.4 Å^3) localities. This ~10 Å^3 difference is in accord with the results of Vezzalini et al. (1997), who reported an enrichment of the smaller cations Si^{4+} (Al/Si = 0.96) and Ca^{2+} (K/Ca = 0.33), which caused changes primarily in the c-axis (Table 1).

Slight but distinct deviations from the almost linear trends of c and γ can be observed in the range 325–350 K (N_2) and 400–450 K (air), with a significant decrease in c and an increase in γ, resulting in a step-wise reduction of the unit-cell volume (Fig. 3c). The other unit-cell parameters are virtually constant, $a \approx b \approx 9.21$ Å, and $|\alpha - \beta|$ decreases (Figs. 3a and 3b). Under higher $p(H_2O)$ conditions, this discontinuity (375–400 K) coincides quite well with the observed increase in extinction angle measured with the polarizing microscope from 353–393 K (Fig. 1).

Optical investigations (Fig. 1) suggest that the triclinic-to-rhombohedral phase transition occurs at 453(1) K and are in good agreement with the results in air (450 and 475 K). As pointed out above, measurement in dry N_2 considerably reduces this range to 350–375 K. The unit-cell parameters above the phase transition ($a \approx 9.37$ Å, $\alpha \approx 91.35°$) are in accord with the extrapolated trends of c and γ. The other parameters exhibit sudden positive (a, $b \approx 0.165$ Å) and negative (α, $\beta \approx -1.35°$) changes, with a unit-cell volume increase of ~25 Å^3 indicating a major rearrangement of the structure of *will* (Fig. 3).

Further heating of dehydrated *will* in air at 500 K resulted in a reduction of all unit-cell parameters (Fig. 3) accompanied by an increase in the crystal mosaicity and significant weakening of diffraction intensities. Holding the crystal at 500 K for 2 h or increasing the temperature to 525 K caused complete amorphization of *will*. This low thermal stability is in contrast to chabazite, which is reported to be stable up to 1073 K (Gottardi and Galli 1985). Differences between the unit-cell parameters determined in the crystal structure analysis (Table 2) and values from the cooling and heating experiments (Table 1; Fig. 3) are likely due to minor differences in $p(H_2O)$ of the two distinct experimental setups.

TABLE 3A. Atomic coordinates and site definitions for triclinic willhendersonite at room temperature (first line) and 373 K (second line)

Atom	Former designation	*x*	*y*	*z*	U_{eq} (Å^2)	No. of atoms in unit cell
Si11a	Si2	0.3127(1)	0.8942(1)	0.1065(1)	0.0130(3)	2
		0.3117(1)	0.8999(1)	0.1110(1)	0.0154(3)	2
Si11b	Si4	0.1082(1)	0.3443(1)	0.8547(1)	0.0124(3)	2
		0.1114(1)	0.3484(1)	0.8565(1)	0.0149(3)	2
Si11c	Si6	0.8504(1)	0.1035(1)	0.3398(1)	0.0130(3)	2
		0.8509(1)	0.1025(1)	0.3398(1)	0.0147(3)	2
Al12a	Al1	0.3432(1)	0.0926(1)	0.8508(1)	0.0128(1)	2
		0.3463(1)	0.0965(1)	0.8525(1)	0.0152(3)	2
Al12b	Al5	0.8886(1)	0.3130(1)	0.0907(1)	0.0130(3)	2
		0.8924(1)	0.3109(1)	0.0921(1)	0.0156(3)	2
Al12c	Al3	0.0905(1)	0.8476(1)	0.3424(1)	0.0126(3)	2
		0.0895(1)	0.8470(1)	0.3430(1)	0.0153(3)	2
O11	O1A	0.7454(3)	0.2443(3)	0.9851(3)	0.0185(7)	2
		0.7517(3)	0.2362(3)	0.9842(3)	0.0234(7)	2
O12	O1B	0.6930(3)	0.0565(3)	0.2683(3)	0.0173(7)	2
		0.6924(3)	0.0555(3)	0.2649(3)	0.0203(7)	2
O13	O1C	0.9740(3)	0.3157(3)	0.7390(3)	0.0160(7)	2
		0.9738(3)	0.3151(3)	0.7442(3)	0.0193(7)	2
O21	O2A	0.1529(3)	0.5125(3)	0.8497(3)	0.0187(7)	2
		0.1578(3)	0.5169(3)	0.8502(3)	0.0228(7)	2
O22	O2B	0.4753(3)	0.8617(3)	0.1663(3)	0.0188(7)	2
		0.4725(3)	0.8616(3)	0.1723(4)	0.0239(7)	2
O23	O2C	0.8277(3)	0.1878(3)	0.4915(3)	0.0166(7)	2
		0.8245(3)	0.1866(3)	0.4919(3)	0.0211(7)	2
O31	O3A	0.2493(3)	0.2505(3)	0.8179(3)	0.0172(7)	2
		0.2526(3)	0.2543(3)	0.8196(3)	0.0193(7)	2
O32	O3B	0.9366(3)	0.2099(3)	0.2381(3)	0.0173(7)	2
		0.9417(3)	0.2056(3)	0.2386(3)	0.0203(7)	2
O33	O3C	0.7864(3)	0.0641(3)	0.7602(3)	0.0182(7)	2
		0.7884(3)	0.0559(3)	0.7562(3)	0.0217(7)	2
O41	O4A	0.0569(3)	0.3044(3)	0.0110(3)	0.0175(7)	2
		0.0633(3)	0.3110(3)	0.0162(3)	0.0214(7)	2
O42	O4B	0.3054(3)	0.0438(3)	0.0209(3)	0.0187(7)	2
		0.3122(3)	0.0509(3)	0.0267(3)	0.0227(7)	2
O43	O4C	0.0574(3)	0.0410(3)	0.6366(3)	0.0169(7)	2
		0.0614(3)	0.0450(3)	0.6340(3)	0.0201(7)	2
Ca1	X1	0.2002(1)	0.2008(1)	0.2038(1)	0.0162(3)	1.964(9)
		0.2048(1)	0.2078(1)	0.2120(1)	0.0201(3)	1.974(9)
K1	X5A	0.4754(8)	0.890(2)	0.4712(8)	0.049(5)	0.46(3)
		0.4781(7)	0.974(1)	0.4832(8)	0.064(2)	0.854(9)
K2	X5B	0.4909(4)	0.4542(3)	0.8534(5)	0.077(1)	1
		0.4928(7)	0.5576(6)	0.140(2)	0.096(5)	0.99(5)
K3	X5C	0.886(1)	0.4882(4)	0.4613(5)	0.060(3)	0.82(2)
		0.491(4)	0.546(4)	0.047(8)	0.11(1)	0.22(5)
OW1	X6C	0.2259(4)	0.4601(4)	0.2606(4)	0.038(1)	2
		0.2281(5)	0.4660(4)	0.2773(5)	0.054(1)	2
OW2	X6B	0.4595(4)	0.2505(4)	0.2399(5)	0.041(1)	2
		0.4675(4)	0.2578(5)	0.2507(5)	0.055(1)	2
OW3	X6A	0.2221(4)	0.2087(4)	0.4583(4)	0.038(1)	2
		0.2398(5)	0.2094(4)	0.4727(4)	0.048(1)	2
OW4	X2A	0.4761(9)	0.784(3)	0.443(1)	0.085(7)	1.54(8)
		0.2957(9)	0.5382(7)	0.5874(8)	0.091(4)	1.64(3)
OW5	X2C	0.763(3)	0.475(1)	0.434(1)	0.073(7)	1.04(6)
		–	–	–	–	–
OW6	–	0.485(5)	0.584(6)	0.436(6)	0.09(3)	0.9(7)
		–	–	–	–	–
OW7	–	0.569(3)	0.489(3)	0.452(3)	0.14(2)	0.74(6)
		–	–	–	–	–

Notes: Atom names correspond to the standardized parameters after Baur and Fischer (2000), former designations refer to the names used by Tillmanns et al. (1984).

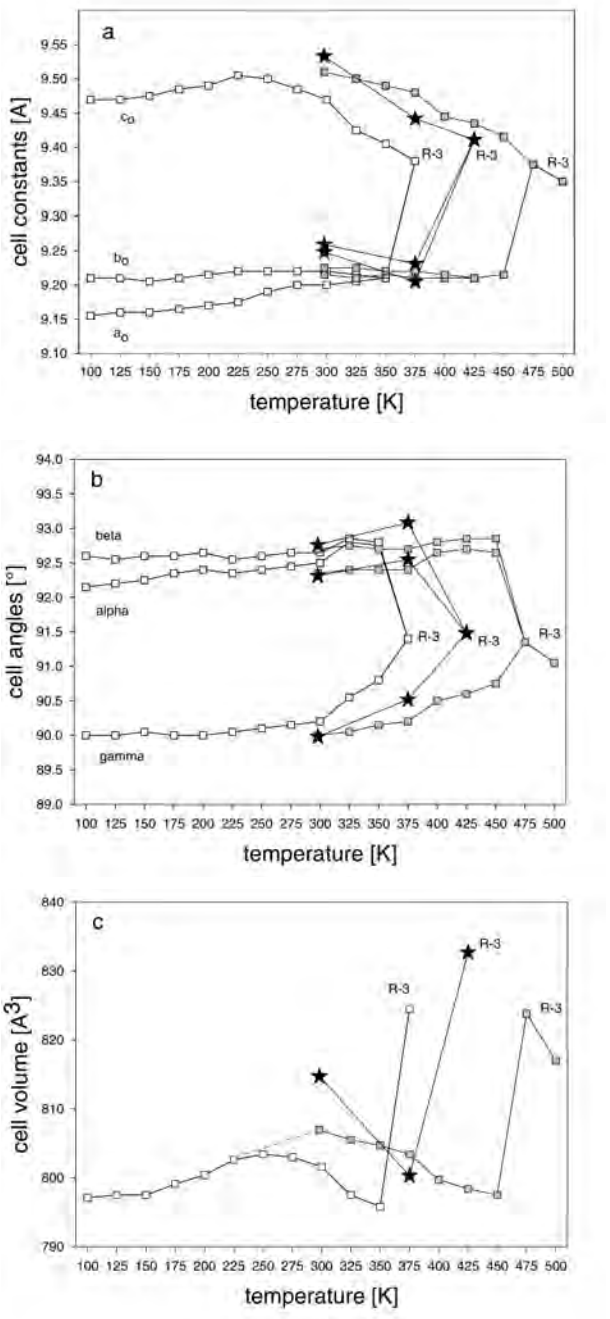

FIGURE 3. Unit-cell parameters as a function of temperature for willhendersonite under dry nitrogen (white squares) from 100 to 375 K (ΔT = 25 ± 1 K) and under humid air (gray squares) from 300 to 500 K (ΔT = 25 ± 5 K). The corresponding values from the crystal structure analyses are marked by black stars.

The triclinic-to-rhombohedral transition observed in the crystal-structure analyses occurs at a temperature between those observed under humid air and under dry nitrogen in the stepwise heating experiments. Al/Si ordering is retained when transforming from $P\bar{1}$ to $R\bar{3}$ symmetry, and transformation to $R\bar{3}m$ is not permitted because it would imply a random distribution of the framework cations. Similar configurations occur in several CHA-type alumino phosphates (see, e.g., SAPO-47, Pluth and Smith 1989, and the compilation of CHA types in Baur and Fischer 2000), which have an ordered distribution of framework P and Al atoms as well.

The chabazite-type framework of willhendersonite belongs to the ABC-6 family of zeolite-type structures with layers of

6-rings (S6R) stacked in an AABBCCAA... sequence as shown in Figure 4. The 6-rings form *hpr* ($4^6 6^2$, Smith 2000) units occupying the vertices of the rhombohedral or triclinic unit cell, enclosing the larger *cha* ($4^6 4^6 6^2 8^6$) units. The *cha* and *hpr* units are linked via common S6R in an alternating sequence forming pillars parallel to [111] and a three-dimensional system of 8-ring channels parallel to the principal axes of the unit cell.

Mean Si-O and Al-O distances (Table 4) range from 1.622 to 1.629 Å and 1.751 to 1.753 Å, respectively, indicating that the framework is essentially built by an ordered arrangement of SiO_4 and AlO_4 tetrahedra forming elliptical double 6-rings (D6R) with the principle axes of the two 6-rings being approximately parallel to each other as shown in Figure 5a. Upon heating beyond the transition temperature, the elliptical rings assume a triangular shape with upper and lower triangles in the D6R being twisted relative to each other by 60° according to its $\bar{3}$ symmetry with the inversion center in the center of the D6R as shown in Figure 5b. Figure 6 shows the transition of the crystal structure with migration of cations and H_2O molecules, with all nonframework positions superimposed irrespective of their real occupancy.

Calcium resides close to the axes through the centers of the D6R about 1.6 Å outside the planes of the single 6-rings of the D6R at room temperature and essentially unchanged at 373 K (Fig. 7a). It is 7-coordinated to four framework O atoms and three H_2O molecules below the transition point. At 423 K, the Ca position splits into three sites (Fig. 7b). Some Ca atoms (Ca1) migrate to the center of D6R forming a distorted, octahedrally coordinated bonding scheme to the O atoms (O4) with three bonds to either side of the single 6-rings of the D6R. The other Ca atoms (Ca2,3) remain outside of D6R with three bonds to the next-nearest O-atoms and two additional long bonds (Ca-O > 3.4 Å) across the 8-ring. This essentially asymmetric 3[+2]-coordination of Ca2 and Ca3 atoms is definitely an unfavorable configuration for Ca in the high-temperature form, which upon rehydraton is assumed to revert to a normal coordination with H_2O molecules as in the triclinic form.

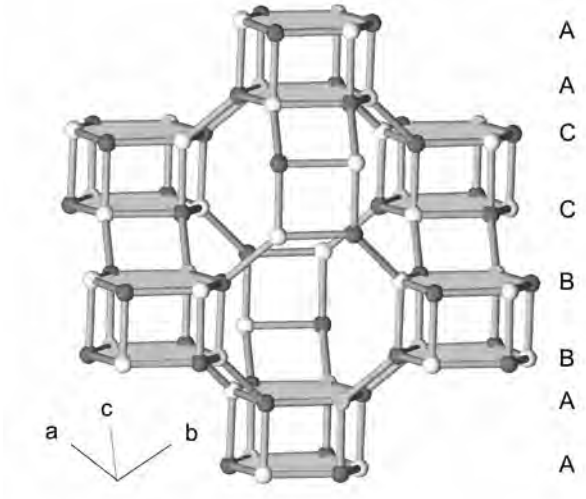

Figure 4. The framework structure of CHA-type *will* with the stacking sequence of single 6-ring layers parallel to rhombohedral [111]. Al atoms are dark; Si atoms are light gray.

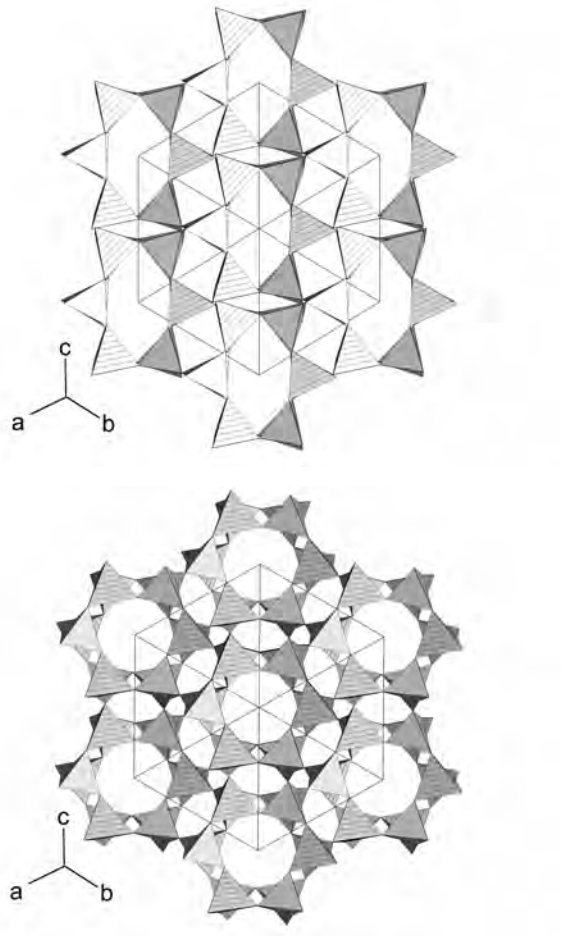

Figure 5. Polyhedral representation of the framework structures of triclinic WIL-RT (**a**) and rhombohedral WIL-423 (**b**) parallel to [111]. AlO_4-tetrahedra are hatched.

Table 3b. Atomic coordinates and site definitions for the rhombohedral high-temperature form of willhendersonite at 423 K

Atom	*x*	*y*	*z*	U_{eq} (Å^2)	Wyckoff position	No. of atoms in unit cell
Si11	0.1002(1)	0.3249(1)	0.8621(1)	0.0222(3)	6*f*	6
Al12	0.3294(1)	0.0830(1)	0.8596(1)	0.0232(3)	6*f*	6
O1	0.2982(3)	0.7098(3)	0.0155(3)	0.0335(7)	6*f*	6
O2	0.1099(3)	0.8731(3)	0.5090(3)	0.0376(8)	6*f*	6
O3	0.2513(3)	0.2479(3)	0.8657(3)	0.0343(7)	6*f*	6
O4	–0.0155(3)	0.0003(3)	0.2545(3)	0.0271(6)	6*f*	6
Ca1	0	0	0	0.0214(7)	1*a*	0.164(2)
Ca2	0.543(1)	0.625(4)	0.011(3)	0.16(1)	6*f*	1.03(9)
Ca3	0.649(3)	0.539(2)	–0.051(3)	0.04(5)	6*f*	0.31(3)
K1	0.5470(8)	0.543(1)	0.017(1)	0.087(3)	6*f*	1.84(8)

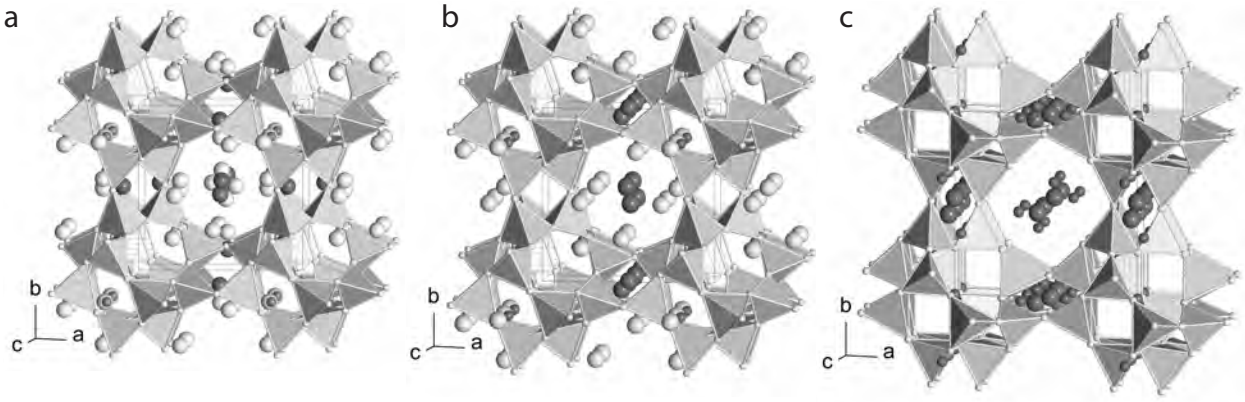

FIGURE 6. Projections of the crystal structures of WIL-RT (**a**), WIL-373 (**b**), and WIL-423 (**c**) approximately parallel to [001] with Ca (dark, small), K (dark, big), and H_2O molecules (light gray, big) drawn as spheres. AlO_4-tetrahedra are hatched.

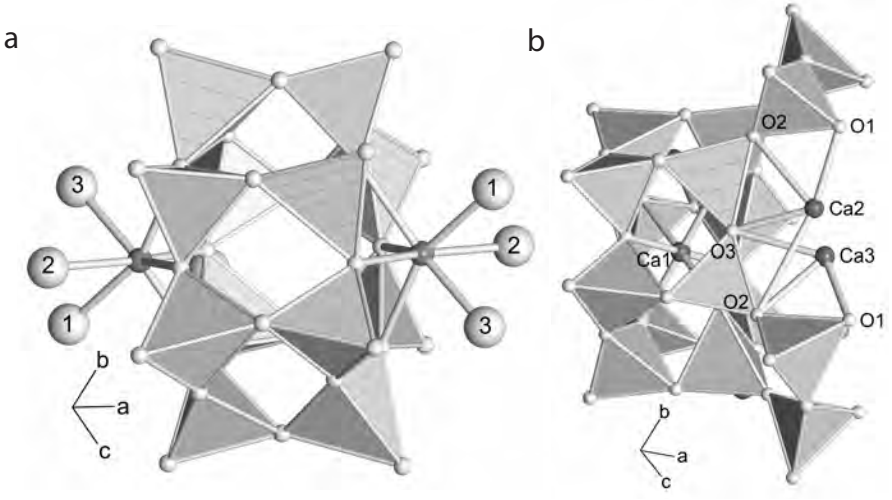

FIGURE 7. The Ca coordination in WIL-RT (**a**) and WIL-423 (**b**). Assignments of atoms and molecules as in Figure 6.

TABLE 4. Selected interatomic distances (Å) and angles (°) for the framework sites in willhendersonite at room temperature (RT), 373, and 423 K

	WIL-RT		WIL-373			WIL-423	
	T-O (Å)	T-O-T (°)	T-O (Å)	T-O-T (°)		T-O (Å)	T-O-T (°)
Si11a-O11	1.600(3)	144.4(2)	1.599(3)	148.2(2)	Si11-O2	1.591(3)	175.1(2)
Si11a-O22	1.615(3)	143.1(2)	1.608(3)	140.2(2)	Si11-O3	1.613(3)	143.2(2)
Si11a-O33	1.636(3)	137.2(2)	1.635(3)	133.8(2)	Si11-O1	1.632(3)	121.6(2)
Si11a-O42	1.636(3)	135.4(2)	1.635(3)	134.7(2)	Si11-O4	1.647(3)	130.2(2)
mean	1.622	140.0	1.619	139.2	mean	1.621	142.5
Si11b-O31	1.612(3)	144.7(2)	1.615(3)	144.8(2)			
Si11b-O21	1.615(3)	144.5(2)	1.614(3)	141.7(2)			
Si11b-O13	1.634(3)	129.8(2)	1.626(3)	131.3(2)			
Si11b-O41	1.642(3)	133.0(2)	1.644(3)	131.7(2)			
mean	1.626	138.0	1.625	137.4			
Si11c-O43	1.604(3)	154.1(2)	1.610(3)	150.8(2)			
Si11c-O12	1.630(3)	126.4(2)	1.634(3)	126.7(2)			
Si11c-O23	1.638(3)	128.7(2)	1.633(3)	127.0(2)			
Si11c-O32	1.642(3)	135.6(2)	1.634(3)	133.9(2)			
mean	1.629	136.2	1.628	134.6			
Al12a-O31	1.732(3)	144.7(2)	1.731(3)	144.8(2)	Al12-O2	1.704(3)	175.1(2)
Al12a-O22	1.748(3)	143.1(2)	1.740(3)	140.2(2)	Al12-O3	1.735(3)	143.2(2)
Al12a-O42	1.753(3)	135.4(2)	1.760(3)	134.7(2)	Al12-O1	1.756(3)	121.6(2)
Al12a-O12	1.773(3)	126.4(2)	1.770(3)	126.7(2)	Al12-O4	1.785(3)	130.2(2)
mean	1.752	137.4	1.750	136.6	mean	1.745	142.5
Al12b-O11	1.730(3)	144.4(2)	1.724(3)	148.2(2)			
Al12b-O21	1.740(3)	144.5(2)	1.732(3)	141.7(2)			
Al12b-O41	1.765(3)	133.0(2)	1.763(3)	131.7(2)			
Al12b-O32	1.769(3)	135.6(2)	1.768(3)	133.9(2)			
mean	1.751	139.4	1.747	138.9			
Al12c-O43	1.724(3)	154.1(2)	1.735(3)	150.8(2)			
Al12c-O33	1.759(3)	137.2(2)	1.765(3)	133.8(2)			
Al12c-O13	1.762(3)	129.8(2)	1.755(3)	131.3(2)			
Al12c-O23	1.765(3)	128.7(2)	1.751(3)	127.0(2)			
mean	1.753	137.5	1.752	135.7			

TABLE 5. Selected interatomic distances for the nonframework sites in willhendersonite at room temperature (RT), 373, and 423 K

	WIL-RT	WIL-373		WIL-423		WIL-RT	WIL-373
Ca-OW3	2.423(4)	2.464(4)	Ca1-O4 6×	2.403(3)	K2-OW6	2.78(5)	
Ca-O41	2.442(3)	2.438(3)	Ca2-O1	2.46(1)	K2-O31	2.923(4)	2.902(6)
Ca-OW2	2.448(4)	2.463(4)	Ca2-O3	2.50(2)	K2-O22	2.941(4)	2.819(6)
Ca-OW1	2.449(4)	2.440(4)	Ca2-O2	2.76(3)	K2-OW2	2.952(5)	3.013(10)
Ca-O42	2.462(3)	2.475(3)	[Ca2-O2	3.43(2)]	K2-OW7	3.00(3)	
Ca-O32	2.476(3)	2.448(3)	[Ca2-O1	3.53(3)]	K2-OW1	3.003(5)	2.956(12)
Ca-O33	2.493(3)	2.466(3)	Ca3-O1	2.44(2)	K2-O21	3.171(4)	3.292(6)
			Ca3-O2	2.59(2)	K2-O11	3.287(4)	3.172(10)
			Ca3-O3	2.75(2)	K2-OW4		3.30(2)
			[Ca3-O1	3.76(2)]			
			[Ca3-O4	3.82(2)]	K3-OW5	1.16(2)*	
					K3-O23	2.862(5)	
K1-OW4	1.01(3)*		K1-O1	2.83(1)	K3-OW1	2.915(7)	3.43(6)
K1-OW6	2.84(5)		K1-O1	2.85(1)	K3-OW7	2.93(3)	
K1-O22	2.908(8)	3.066(9)	K1-O3	2.88(1)	K3-O21	2.969(6)	3.39(4)
K1-O23	2.936(9)	3.167(7)	K1-O2	3.19(1)	K3-O13	3.022(7)	
K1-OW3	3.00(1)	3.106(9)	K1-O2	3.46(1)	K3-OW3	3.061(6)	
K1-O12	3.018(8)	2.940(8)			K3-O13	3.217(6)	
K1-OW4	3.12(3)				K3-O32	3.322(5)	
K1-OW2	3.13(1)	3.389(10)			K3-OW5	3.36(2)	
K1-O33	3.236(8)	3.246(7)			K3-O11		3.03(3)
K1-O12	3.28(1)	3.043(8)			K3-O22		3.11(4)
K1-OW3		3.129(8)			K3-O31		3.16(4)
					K3-OW2		3.36(5)
					K3-OW2		3.45(7)
					K3-O21		3.50(5)

* Distances marked by an asterisk are avoided by partial occupancies.

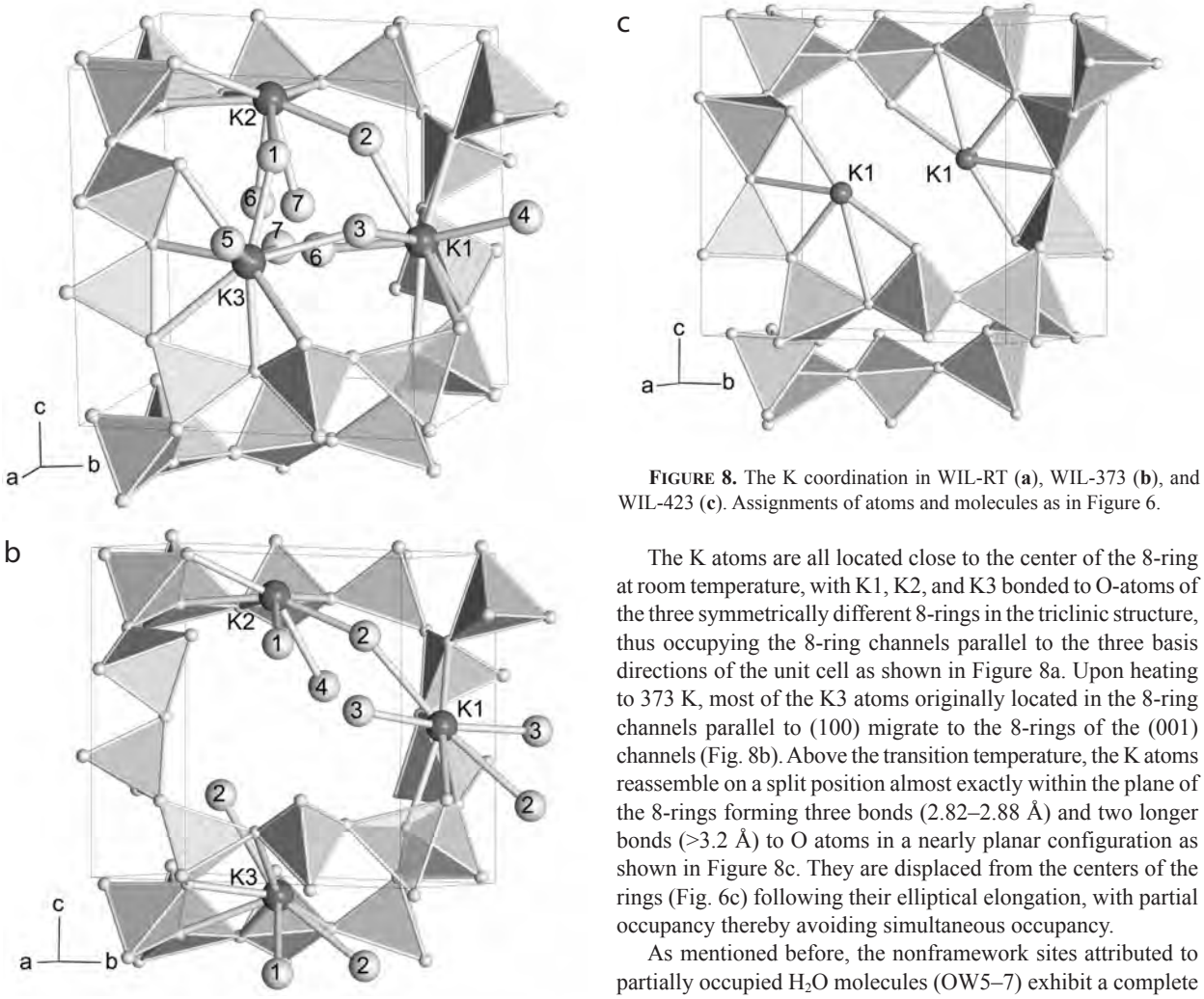

FIGURE 8. The K coordination in WIL-RT (**a**), WIL-373 (**b**), and WIL-423 (**c**). Assignments of atoms and molecules as in Figure 6.

The K atoms are all located close to the center of the 8-ring at room temperature, with K1, K2, and K3 bonded to O-atoms of the three symmetrically different 8-rings in the triclinic structure, thus occupying the 8-ring channels parallel to the three basis directions of the unit cell as shown in Figure 8a. Upon heating to 373 K, most of the K3 atoms originally located in the 8-ring channels parallel to (100) migrate to the 8-rings of the (001) channels (Fig. 8b). Above the transition temperature, the K atoms reassemble on a split position almost exactly within the plane of the 8-rings forming three bonds (2.82–2.88 Å) and two longer bonds (>3.2 Å) to O atoms in a nearly planar configuration as shown in Figure 8c. They are displaced from the centers of the rings (Fig. 6c) following their elliptical elongation, with partial occupancy thereby avoiding simultaneous occupancy.

As mentioned before, the nonframework sites attributed to partially occupied H_2O molecules (OW5–7) exhibit a complete

loss of H_2O at 373 K, whereas the almost fully occupied H_2O sites (OW1–4) remain stable up to the phase transition temperature. Changes in the H_2O positions are shown in Figure 6 and can be inferred from the cation coordinations shown in Figures 7 and 8.

Summarizing, the transition of willhendersonite from triclinic to rhombohedral symmetry upon dehydration can be attributed to cation migrations partly to low-coordinated sites, causing a relaxation of the elliptically deformed 6-rings of TO_4 tetrahedra to a more circular shape. In contrast to chabazite, which has the same framework topology but disordered T atoms, the 6-rings in the D6R units are twisted relative to each other in the high temperature form. The transition temperature strongly depends on the degree of humidity, ranging from 375 K in dry nitrogen to 475 K in humid air. Upon rehydration, the crystals are polysynthetically twinned, thus preventing single-crystal studies of the reconverted zeolite.

ACKNOWLEDGMENTS

We thank G. Giester and M.A. Götzinger (Wien, Austria) for their support during the single-crystal data collection and scanning electron microscopy investigations, respectively, and David Bish for his substantial comments on the manuscript. This work was supported by the "Kommission für Grundlagen der Mineralrohstoffforschung" of the Austrian Academy of Sciences, and by the International Centre for Diffraction Data (Newtown Square, Pennsylvania, U.S.A.) through Grant-in-Aid 90-03.

REFERENCES CITED

Akizuki, M. (1981) Origin of optical variation in chabazite. Lithos 14, 17–21.

Baerlocher, C. and McCusker, L.B. (2007) Database of Zeolite Structures, published by the International Zeolite Association, hosted at Lab. Crystallography, ETH Zürich, Switzerland, http://www.iza-structure.org/databases/.

Baur, W.H. and Fischer, R.X. (2000) Zeolite-type crystal structures and their chemistry. In W.H. Baur and R.X. Fischer, Eds., Landolt-Börnstein, Numerical Data and Functional Relationships in Science and Technology, New Series, Group IV: Physical Chemistry, Volume 14, Microporous and other framework materials with zeolite-type structures, Subvolume B, 459 p. Springer-Verlag, Berlin.

Becke, F. (1880) Über die Zwillingsbildung und die optischen Eigenschaften des Chabasit. Tschermaks Mineralogisch-Petrographische Mitteilungen 2, 391–418.

Bennett, J.M. and Marcus, B.K. (1988) The crystal structures of several metal aluminophosphate molecular sieves. In P.J. Grobet and W.J. Mortier, Eds., Innovation in Zeolite Materials Science, 37, p. 269–279. Studies in Surface Science and Catalysis, Elsevier, Amsterdam.

Birkenstock, J., Messner, T., and Fischer, R.X. (2007) BRASS, the Bremen Rietveld Analysis and Structure Suite. Universität Bremen, Germany.

Cosier, J. and Glazer, A.M. (1986) A nitrogen-gas-stream cryostat for general X-ray diffraction studies. Journal of Applied Crystallography, 19, 105–107.

Feng, P., Bu, X., and Stucky, G.D. (1997) Hydrothermal syntheses and structural characterization of zeolite analogue compounds based on cobalt phosphate. Nature 388, 735–741.

Fischer, R.X. and Messner, T. (2007) STRUPLO: A drawing program for crystal structures. Universität Bremen, Germany.

Gottardi, G. and Galli, E. (1985) Natural Zeolites. Springer-Verlag, Berlin.

Harding, M.M. and Kariuki, B.M. (1994) Microcrystal structure determination of $AlPO_4$-CHA using synchrotron radiation. Acta Crystallographica, C50, 852–854.

Mazzi, F. and Galli, E. (1983) The tetrahedral framework of chabazite. Neues Jahrbuch für Mineralogie, Monatshefte, 1983, 461–480.

Oliver, S., Kuperman, A., Lough, A., and Ozin, G.A. (1997) Synthesis and characterization of a fluorinated anionic aluminophosphate framework UT-6, and its high-temperature dehydrofluorination to $AlPO_4$-CHA. Journal of Materials Chemistry 7, 807–812.

Peacor, R.D., Dunn, P.J., Simmons, W.B., Tillmanns, E., and Fischer, R.X. (1984) Willhendersonite, a new zeolite isostructural with chabazite. American Mineralogist, 69, 186–189.

Pluth, J.J. and Smith, J.V. (1989) Silicoaluminophosphate with encapsulated methylbutylamine species: Chabazite structure, charge coupling between framework and inferred ammonium species, and severe molecular disorder. Journal of Physical Chemistry, 93, 6516–6520.

Schott-Darie, C., Kessler, H., Soulard, M., Gramlich, V., and Benazzi, E. (1994) Diversity of the system Ga_2O_3-P_2O_5-H_2O-HF in the presence of organic species. In J. Weitkamp, H.G. Karge, H. Pfeifer, and W. Hölderich, Eds., Zeolites and Related Microporous Materials: State of the Art 1994, 84, p. 101–108. Studies in Surface Science and Catalysis, Elsevier, Amsterdam.

Shannon, R.D. (1976) Revised effective ionic radii and systematic studies of interatomic distances in halides and chalcogenides. Acta Crystallographica, A32, 751–767.

Sheldrick, G. (1997) SHELXL-97, a computer program for crystal structure refinement. University of Göttingen, Germany.

Sieber, N.H.W. (1989) Kristallchemische Untersuchungen natürlicher Zeolithe: Lithium-Austausch in Natrolith, Phasenumwandlung in Willhendersonit. Dissertation, University of Würzburg, Germany.

Simmen, A. (1992) Beitrage zur Kristallchemie mikroporöser Alumino-und Gallophosphate. Dissertation, ETH, Zürich.

Smith, J.V. (2000) Tetrahedral frameworks of zeolites, clathrates and related materials. In W.H. Baur and R.X. Fischer, Eds., Landolt-Börnstein, Numerical Data and Functional Relationships in Science and Technology, New Series, Group IV: Physical Chemistry, Volume 14, Microporous and other framework materials with zeolite-type structures, Subvolume A, 266 p. Springer-Verlag, Berlin.

Smith, J.V., Knowles, C.R., and Rinaldi, F. (1964) Crystal structures with a chabazite framework. III. Hydrated Ca-chabazite at +20 and –150 °C. Acta Crystallographica, 17, 374–384.

Tillmanns, E. and Fischer, R.X. (1982) Über ein neues Zeolithmineral mit geordnetem Chabasitgerüst. Zeitschrift für Kristallographie 159, 125–126.

Tillmanns, E., Fischer, R.X., and Baur W.H. (1984) Chabazite-type framework in the new zeolite willhendersonite, $KCaAl_3Si_3O_{12}\cdot 5H_2O$. Neues Jahrbuch für Mineralogie, Monatshefte, 1984, 547–558.

Tuinstra, F. and Fraase-Storm, G. M. (1978) A universal high-temperature device for single-crystal diffraction. Journal of Applied Crystallography, 11, 257–259.

van Reeuwijk, L.P. (1974) The thermal dehydration of natural zeolites, 88 p. Veenman and Zonen, Wageningen.

Vezzalini, G., Quartieri, S., and Galli, E. (1997) Occurrence and crystal structure of a Ca-pure willhendersonite. Zeolites, 19, 75–79.

Walter, F. and Postl, W. (1984) Willhendersonit vom Stradner Kogel, südlich Gleichenberg, Steiermark. Mitteilungen der Abteilung für Mineralogie am Landesmuseum Joanneum, 52, 39–43.

Wilson, A.J.C. (1992) International Tables for Crystallography, Volume C: Mathematical, physical and chemical tables. Kluwer Academic Publishers, Dordrecht.

MANUSCRIPT RECEIVED JULY 20, 2007
MANUSCRIPT ACCEPTED JANUARY 23, 2008
MANUSCRIPT HANDLED BY PRZEMYSLAW DERA